

AutoPET Challenge 2023: Sliding Window-based Optimization of U-Net

Matthias Hadlich^{1,*}, Zdravko Marinov^{1,2,*}, and Rainer Stiefelhagen¹

¹ Institute for Anthropomatics and Robotics, Karlsruhe Institute of Technology, Karlsruhe, Germany

matthias.hadlich@student.kit.edu, {zdravko.marinov, rainer.stiefelhagen}@kit.edu

² HIDSS4Health - Helmholtz Information and Data Science School for Health, Karlsruhe/Heidelberg, Germany

Abstract. Tumor segmentation in medical imaging is crucial and relies on precise delineation. Fluorodeoxyglucose Positron-Emission Tomography (FDG-PET) is widely used in clinical practice to detect metabolically active tumors. However, FDG-PET scans may misinterpret irregular glucose consumption in healthy or benign tissues as cancer. Combining PET with Computed Tomography (CT) can enhance tumor segmentation by integrating metabolic and anatomic information. FDG-PET/CT scans are pivotal for cancer staging and reassessment, utilizing radiolabeled fluorodeoxyglucose to highlight metabolically active regions. Accurately distinguishing tumor-specific uptake from physiological uptake in normal tissues is a challenging aspect of precise tumor segmentation. The AutoPET challenge addresses this by providing a dataset of 1014 FDG-PET/CT studies, encouraging advancements in accurate tumor segmentation and analysis within the FDG-PET/CT domain. Code: <https://github.com/matt3o/AutoPET2-Submission/>

Keywords: Semantic Segmentation · Sliding Window · U-Net

1 Introduction

In the domain of oncological diagnostics, the integration of Fluorodeoxyglucose Positron-Emission Tomography (FDG-PET) and Computed Tomography (CT) has assumed a pivotal role, facilitating comprehensive insights into the metabolic dynamics of various malignant solid tumor entities [1]. FDG-PET, acknowledged for its capacity to delineate glucose consumption within tissues, holds significant promise in therapy control and monitoring, owing to the characteristic escalated glucose uptake by tumor lesions [3]. However, the non-specificity of FDG-PET often introduces interpretational ambiguities, as it may also manifest in benign or healthy tissue [6], potentially leading to erroneous diagnoses.

To mitigate this diagnostic challenge, the fusion of PET with CT has emerged as an integrated approach, combining metabolic data with precise anatomical

* Shared first author

information. This combination enhances tumor detection accuracy [1], [13], offering a cohesive synergy particularly valuable in clinical practice [6].

Within this evolving landscape of medical diagnostics, the Automatic Lesion Segmentation in Whole-Body FDG-PET/CT Challenge (AutoPET)³ embodies a critical juncture. It motivates researchers and practitioners to develop automated, bi-modal methodologies for the three-dimensional segmentation of tumor lesions embedded within FDG-PET and CT scans [6]. The challenge accelerates advancements in deep learning-based automated tumor lesion segmentation through the provision of a large densely annotated dataset of 1014 volumes.

In this work, we propose using the well-known U-Net architecture [15] to tackle the AutoPET challenge. Despite the ubiquity of U-Net models in medical segmentation tasks [9], [4], achieving high performance in the domain of whole-body PET/CT lesion segmentation has remained elusive [12], [17], [8], [16], [7] largely due to the scarcity of training data in preceding studies [3]. Drawing upon the insights provided by the AutoPET Challenge U-Net-based winner from 2022 [16], we undertake a practical investigation to understand the important training parameters of the U-Net model for segmenting lesions. We believe that it is possible to achieve a better and more robust model by focusing on the intricacies of data pre-processing, data augmentation, learning rate scheduling, and crop-size selection during model training. Our work and model are based on prior experiments in interactive segmentation [14]. Thus, for our hyperparameter tuning experiments, we present results using our interactive model. Nonetheless, for our final submission, we exclude the integration of interactive clicks into the model and employ its optimal hyperparameter configuration.

2 Methodology

2.1 Model Architecture

The model used for the challenge is called DynUNet, which is an adaption of the UNet for the MONAI library [2]. Contrary to the default UNet, DynUNet does not use max-pooling for downsampling but instead uses strided convolutions. Additionally, the residual is passed through a convolutional layer such that the input size from the downsampling layer matches the output size of this layer. All of the changes can be traced back to three prior works: [10], [11], and [5].

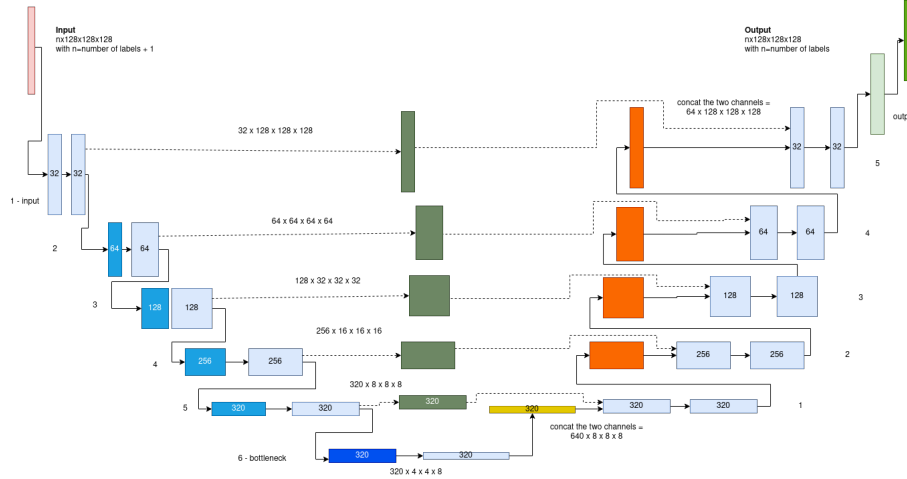
Our default configuration of the network consists of six layers of filter size [32, 64, 128, 256, 320, 320]. As discussed above, the convolutions are strided with a size of [1, 2, 2, 2, 2, [2, 2, 1]], and the upsampling is thus done in the inverse order. An architectural diagram can be found in Figure 1.

2.2 Data Pre-processing and Augmentation

Pre-processing. We restrict ourselves by using only the PET volumes from the paired PET/CT scans. We apply multiple pre-processing transformations to

³ <https://autopet-ii.grand-challenge.org/>

Fig. 1. An overview of the used DynUNet architecture.



each batch of data. Apart from changing the channel order, the orientation is set to a RAS (Right-Anterior-Superior) coordinate system. As the AutoPET spacing is $\approx [2, 2, 3] \text{mm}^3$, the data is resampled accordingly with this fixed voxel size. The intensity of each PET image is scaled based on its voxel intensity statistics with `MONAI::ScaleIntensityRangePercentiled` to the 0.05 and 99.95 percentiles. During training, a random crop of size $224 \times 224 \times 224$ is sampled, with a probability of 0.6 of being centered around a tumor lesion and 0.4 of being centered around the background. To achieve this, we utilize the `RandCropByPosNegLabeld` MONAI transform. This crop is balanced by the class label of the voxel in the crop's center - in 60% of the cases the voxel is positive, and in the other 40% it is negative. This ensures that the network learns about positive and negative samples in a more balanced training regime.

Data Augmentation. We apply two types of data augmentation - random flipping and random rotation. We apply a random flip on each spatial axis with a probability of 0.1. We also apply a random 90-degree rotation with a probability of 0.1 for each axis.

2.3 Data Post-processing

Since we are using a sliding window approach, the final prediction volume gets stitched from the various output patches. This process is done with a user defined overlap, in our case this was set to 75%.

After the result prediction a softmax is applied.

For the ensemble based solution the two steps mentioned above are done for each of the five networks prediction separately. After the softmax on each

prediction a voting mechanism combines the different predictions into a single one.

2.4 Hyperparameter Tuning

As explained above most of the different experiments have been run on interactive code. Nevertheless they should be representative in terms of general performance of the network. Variations of $\pm 0.5\%$ Dice are to be expected since the guidance signal was non-deterministic.

Sliding window versus normal inferer First of all we compare the sliding window inference to the normal one, figure 2.4. As it can be seen in the table, on the interactive code the sliding window inferer wins with a lead of 2.81% Dice.

Next different region of interest sizes have been tried out. The best performing one here was the $128 \times 128 \times 128$ crop. Note that the sliding window was active during training. In the thesis it is shown that training with overlap active gains about 1% of Dice.

This overlap means for the $128 \times 128 \times 128$ instead a window of size $320 \times 320 \times 320$ has been calculated, with calculations being equal to a normal inferer of size $384 \times 384 \times 384$. As we can see a lot of overhead calculations are being done by the sliding window inferer. However in the next subsection we will show that the overhead calculations for the overlap actually lead to a better Dice score.

Table 1. Interactive run of Sliding Window versus Simple Inferer

	Sliding Window	Simple Inferer
Dice	83.83%	81.02%

Table 2. Different region of interest sizes compared. Trained on a crop of size $256 \times 256 \times 256$.

	64x64x64	128x128x128	192x192x192	256x256x256
Dice (validation)	84.74%	85.22%	83.66%	84.75%
Dice (training)	87.99%	88.46%	88.98%	88.79%

Sliding window overlap Now we will look at the overlap of the sliding window inferer. Table 2.4 shows that increasing the overlap also increases the Dice score of the network. In our experiments the higher the overlap the better the results have been. This can be seen as a way of creating a mini Ensemble with same

weights. The overlap uses a Gaussian fade away to make the regions closer the center weight more heavily when stitching together the final output.

Additionally experiments have been run to verify the impact of training with overlap on. Table 4, which shows a network trained on 0% overlap, overall shows slightly worse results, especially for the higher overlaps it becomes significant. As expected running it with 0 overlap returns slightly better results than the network trained with overlap being forced to use none. We can thus conclude that activating overlap during training enhances the final score.

Table 3. Non-interactive validation runs with different settings for the overlap. The network has been trained on 25% overlap.

Experiment	Overlap	Dice
201	0	66.33%
202	0.25	73.04%
203	0.5	73.54%
207	0.75	74.07%

Table 4. Non-interactive validation runs with different settings for the overlap. The network has been trained on 0% overlap.

Experiment	Overlap	Dice
v_208_0.0	0	66.57%
v_208_0.25	0.25	71.35%
v_208_0.5	0.5	71.99%
v_208_0.75	0.75	72.86%

Convergence behaviour with different losses Figure 2 shows the convergence behaviour of the Dice loss vs the DiceCELoss. As it can be seen the DiceCELoss start with a higher initial validation Dice in epoch 10, 73.62% against 70.09%. Also the final Dice metric was a little bit higher, 85.47% for DiceCELoss and 84.62% for Dice loss. However a plateau appears to be reached for both losses. In other experiments with more iterations it was shown that this method can reach a validation Dice of up to 87.60%.

We can thus fully recommend the DiceCELoss as a standard choice for training. It converges faster and also yields higher final scores especially in terms of Dice.

Intensity scaling options Finally a quick comparison of different intensity scaling options. The base run was a pre-calculated batch statistics normalization to the 0.005 and 99.95 percentiles of the intensity. The first ScaleIntensityRangePercentiled applied the same percentiles but this time based on the

statistics of a each item. The last ScaleIntensityRangePercentiled is a base run with no clipping of the intensities, it only normalizes the intensity from 0 to 1.

As we can see the item-wise statistics outperformed the batch-wise statistics and the clipless method.

Table 5. Different ScaleIntensity settings compared.

	Base run CosineAnnealingLr (104)	ScaleIntensity- RangePercentiled (148)	ScaleIntensity- RangePercentiled 2 (149)
Dice	85.63%	86.69%	85.44%

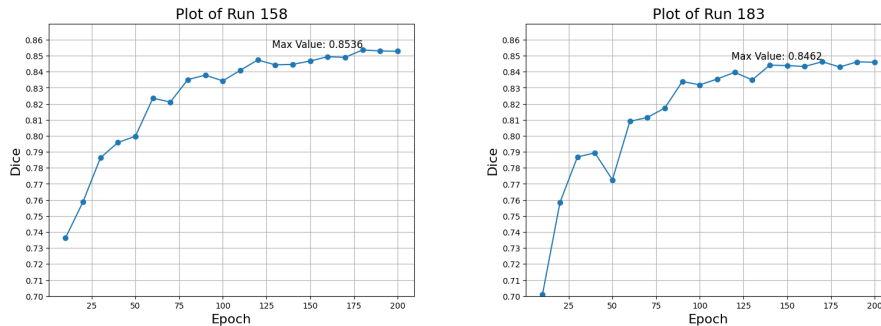
Best parameters A summary of the best found results can be found in table 2.4.

3 Proposed solutions to the AutoPET2 Challenge

We propose two different approaches for the challenge:

- A single network with seven layers as stated above, trained for 800 epochs.
- An cross-validation ensemble of five networks trained on splits of the data. They were trained only without using the validation split. Training was done for N/A epochs. The results of the different networks got combined with an equally weighted voting mechanism. The network themselves are one layer flatter, so contain only six layers. This was mostly done to speed up the training but also to fit the five networks into the GPU memory.

Fig. 2. Comparing the Dice Loss, in MONAI called MeanDice to the DiceCELoss.



(a) Validation Dice of run 158. In this run the DiceCELoss has been used as the loss.

(b) Validation Dice of run 183. In this run the MeanDice has been used as the loss.

Table 6. Best settings

Parameter name	Setting
Network	MONAI DynUNet with [32, 64, 128, 256, 320, 320, 320] filters and a depth of seven layers
Loss	DiceCELoss with squared_pred=False and include_background=True
Optimizer	Adam
Learning rate scheduler	CosineAnnealingLR (initial_lr=2e-4, eta_min=1e-8)
Inferer	Sliding window inferer with ROI size 128x128x128, sliding window overlap 0.75
Intensity scaling with	Custom Scaling to 0.05% and 99.95% intensity percentiles using ScaleIntensityRanged
Automatic Mixed Precision	Active

4 Results

Method	Train dice	Results on the preliminary test set		
		Dice score	False negative volume	False positive volume
Single network	87.43%	56.52%	0.0249	1.8015
Ensemble	N/A	53.82%	0.4678	1.6372

Table 7. The results of our method in the AutoPET2 challenge.

5 Post mortem: NaN errors during training if AMP is active

In the preparation for the challenge we ran into NaN errors when training on A100 GPUs, but only when automated mixed precision was on. During the debugging we found out our input already contained NaNs.

The reason in our case was a training crop to positive / negative areas of size 224x224x224. At the borders of the volume this resulted in crops which contained almost only 0s or even only 0s. Our current hypothesis is that the normalization on the crop produces division by 0 errors. This would make especially sense for the intensity scaling which might degrade if the input tensor only contains 0s. However more debugging is necessary to find out the exact transform which produces the NaN errors.

The solution is to add a filter after the pre-transform to remap all NaN values to 0. In our case this fixed the problem and we could resume training with AMP on the A100 GPUs.

6 Acknowledgment

The present contribution is supported by the Helmholtz Association under the joint research school “HIDSS4Health – Helmholtz Information and Data Science School for Health“. This work was performed on the HoreKa supercomputer funded by the Ministry of Science, Research and the Arts Baden-Württemberg and by the Federal Ministry of Education and Research.

References

1. Ben-Haim, S., Ell, P.: 18f-fdg pet and pet/ct in the evaluation of cancer treatment response. *Journal of Nuclear Medicine* **50**(1), 88–99 (2009)
2. Cardoso, M.J., Li, W., Brown, R., Ma, N., Kerfoot, E., Wang, Y., Murrey, B., Myronenko, A., Zhao, C., Yang, D., et al.: Monai: An open-source framework for deep learning in healthcare. *arXiv preprint arXiv:2211.02701* (2022)
3. Egger, J., Gsaxner, C., Pepe, A., Pomykala, K.L., Jonske, F., Kurz, M., Li, J., Kleesiek, J.: Medical deep learning—a systematic meta-review. *Computer Methods and Programs in Biomedicine* p. 106874 (2022)
4. Eisenmann, M., Reinke, A., Weru, V., Tizabi, M.D., Isensee, F., Adler, T.J., Ali, S., Andrearczyk, V., Aubreville, M., Baid, U., et al.: Why is the winner the best? In: *Proceedings of the IEEE/CVF Conference on Computer Vision and Pattern Recognition*. pp. 19955–19966 (2023)
5. Futrega, M., Milesi, A., Marcinkiewicz, M., Ribalta, P.: Optimized u-net for brain tumor segmentation. In: *International MICCAI Brainlesion Workshop*. pp. 15–29. Springer (2021)
6. Gatidis, S., Früh, M., Fabritius, M., Gu, S., Nikolaou, K., La Fougère, C., Ye, J., He, J., Peng, Y., Bi, L., et al.: The autopet challenge: Towards fully automated lesion segmentation in oncologic pet/ct imaging (2023)
7. Hallitschke, V.J., Schlumberger, T., Kataliakos, P., Marinov, Z., Kim, M., Heiliger, L., Seibold, C., Kleesiek, J., Stiefelhagen, R.: Multimodal interactive lung lesion segmentation: A framework for annotating pet/ct images based on physiological and anatomical cues. *arXiv preprint arXiv:2301.09914* (2023)
8. Heiliger, L., Marinov, Z., Hasin, M., Ferreira, A., Fragemann, J., Pomykala, K., Murray, J., Kersting, D., Alves, V., Stiefelhagen, R., et al.: Autopet challenge: Combining nn-unet with swin unetr augmented by maximum intensity projection classifier. *arXiv preprint arXiv:2209.01112* (2022)
9. Isensee, F., Jaeger, P.F., Kohl, S.A., Petersen, J., Maier-Hein, K.H.: nnu-net: a self-configuring method for deep learning-based biomedical image segmentation. *Nature methods* **18**(2), 203–211 (2021)
10. Isensee, F., Jäger, P.F., Kohl, S.A., Petersen, J., Maier-Hein, K.H.: Automated design of deep learning methods for biomedical image segmentation. *arXiv preprint arXiv:1904.08128* (2019)
11. Isensee, F., Petersen, J., Klein, A., Zimmerer, D., Jaeger, P.F., Kohl, S., Wasserthal, J., Koehler, G., Norajitra, T., Wirkert, S., et al.: nnu-net: Self-adapting framework for u-net-based medical image segmentation. *arXiv preprint arXiv:1809.10486* (2018)
12. Liu, Z., Zhong, S., Mo, J.: Autopet challenge 2022: Step-by-step lesion segmentation in whole-body fdg-pet/ct. *arXiv preprint arXiv:2209.09199* (2022)

13. Marinov, Z., Reiß, S., Kersting, D., Kleesiek, J., Stiefelhagen, R.: Mirror u-net: Marrying multimodal fission with multi-task learning for semantic segmentation in medical imaging. arXiv preprint arXiv:2303.07126 (2023)
14. Marinov, Z., Stiefelhagen, R., Kleesiek, J.: Guiding the guidance: A comparative analysis of user guidance signals for interactive segmentation of volumetric images. arXiv preprint arXiv:2303.06942 (2023)
15. Ronneberger, O., Fischer, P., Brox, T.: U-net: Convolutional networks for biomedical image segmentation. In: Medical Image Computing and Computer-Assisted Intervention—MICCAI 2015: 18th International Conference, Munich, Germany, October 5-9, 2015, Proceedings, Part III 18. pp. 234–241. Springer (2015)
16. Ye, J., Wang, H., Huang, Z., Deng, Z., Su, Y., Tu, C., Wu, Q., Yang, Y., Wei, M., Niu, J., et al.: Exploring vanilla u-net for lesion segmentation from whole-body fdg-pet/ct scans. arXiv preprint arXiv:2210.07490 (2022)
17. Zhong, S., Mo, J., Liu, Z.: Autopet challenge 2022: Automatic segmentation of whole-body tumor lesion based on deep learning and fdg pet/ct. arXiv preprint arXiv:2209.01212 (2022)